Analytic theory of relativistic self-focusing for a Gaussian light beam entering a plasma: Renormalization-group approach

V. F. Kovalev[1,2] and V. Yu. Bychenkov[3,2]

[1]*Keldysh Institute of Applied Mathematics, Russian Academy of Sciences, Moscow 125047, Russia*

[2]*Center for Fundamental and Applied Research, Dukhov Research Institute of Automatics (VNIIA), Moscow 127055, Russia*

[3]*P. N. Lebedev Physics Institute, Russian Academy of Sciences, Moscow 119991, Russia*

(Received 6 December 2018; published 2 April 2019)

Using the renormalization-group approach, we consider an analytic theory describing the formation of a self-focusing structure of a laser beam in a plasma with relativistic nonlinearity for a given radial intensity distribution at the entrance and derive approximate analytic solutions. We study three stationary self-focused waveguide propagation modes with respect to controlling laser-plasma parameters for a Gaussian radial intensity distribution at the plasma boundary. The proposed theory specifies the domains and their boundaries on the plane of the controlling parameters where (1) self-trapping, (2) self-focusing on the axis, and (3) tubular self-focusing solutions occur. We review the concept of the critical power and show that it must be correlated to the form of the entering light pulse and its value corresponding to the minimum power that admits self-channeling can be significantly lower than the widely used value $17(\omega^2/\omega_{pe}^2)$ GW.

DOI: 10.1103/PhysRevE.99.043201

I. INTRODUCTION

When investigating the propagation of powerful laser radiation beams in plasma, a key issue is to find conditions for transferring the energy of laser radiation to distances exceeding the length at which its natural diffraction spreading occurs in a linear medium. The diffraction divergence of a light beam in a nonlinear medium (plasma) can be prevented due to a well-known self-focusing effect for high-power laser radiation. For the first time self-focusing was predicted by Askar'yan in 1962 [1] due to the thermal and charge-displacement nonlinearities. Lasers now have an intensity for which the problem of the self-focusing of light in a plasma with a relativistic nonlinearity becomes relevant. An importance of relativistic effects for self-focusing was first claimed in [2], and then in [3]. Standardly, relativistic self-focusing is associated with the effects of relativistic electron mass and charge-displacement self-channeling that was analyzed theoretically in the works [4,5] and later on was observed experimentally [6]. Then, it was studied more completely in both experiments and numerical simulations in Refs. [7–9]. A more complicated physical picture may occur if a self-generated magnetic field affects a relativistic self-focusing. This was first studied both theoretically and numerically [10] and then supported by experiment with simulation [11]. Clarifying the nature of the self-focusing process helps to introduce various applications, such as wake-field particle acceleration [12–16], fast ignition concept [17], and penetration of laser radiation through underdense plasma [18].

Analytical description of the relativistic self-focusing is based on the classical nonrelativistic approach developed during the decades of the last century for various types of medium's nonlinearities and models of light propagation [1,19–24]. From the historical standpoint, self-focusing of wave beams for media with a cubic nonlinearity that corresponds to a relatively low beam intensity has been studied extremely thoroughly. The obtained results are represented by exact and approximate analytic theories and also by many numerical calculations. These results have been described in several reviews and monographs [19–24]. As for the relativistic self-focusing, it still remains the subject of active theoretical studies (e.g., [25]). Despite the large number of theoretical investigations performed, they are all far from the most needed study: an analytic description of the formation of a self-focusing structure of a laser beam having a given form of the radial intensity distribution at the entrance. All the theories of relativistic self-focusing so far known that describe the spatial distribution of the electric field of a light beam in a plasma are to some extent based on *ad hoc* constructions, and this does not allow accepting the obtained solutions, their properties, and the resultant parametric scaling as entirely relevant to the boundary value problem (Cauchy problem for the stationary beams) of practical interest. A theory describing the redistribution of the laser beam shape from a given radial distribution at the medium boundary (e.g., from a Gaussian-shaped beam profile) to the self-consistent self-channeling profile is very much needed.

A natural advance in the theory of relativistic self-focusing would be to solve the corresponding Cauchy problem for a plasma where an intense laser beam modifies the dielectric constant due to the effects of both relativistic electron mass and ponderomotive displacement of electrons. We note that a relativistically intense laser beam leads to the displacement of electrons from the plasma channel even to the extent of their complete evacuation, called electron cavitation [5,6,26–29]. We previously presented a solution of the Cauchy problem using our proposed approximate theory for a nonrelativistic plasma with cubic and saturating nonlinearities for a

 ©2019 American Physical Society

Gaussian incoming light beam [30,31]. We recently proposed an extension of this theory based on the renormalization-group approach [32] to a plasma medium with relativistic nonlinearity, but the preliminary study [33] was limited to only a selective demonstration of representative examples for channeled light propagation. Here, we aim to fill the void by extending the Cauchy problem for relativistic self-focusing to a multiparametric study of possible channeled propagation regimes and their domains of existence on the plane of laser-plasma controlling parameters, i.e., electron plasma density, laser intensity ($I \times \lambda^2$, in fact), and beam size. The theory presented here applies to a circularly polarized electromagnetic laser wave and a cold plasma approximation. This analytic study describes self-consistently the formation of self-focusing structures for a relativistically intense laser beam with a given transverse form (e.g., Gaussian) of the intensity distribution at the entrance.

Certainly, numerical simulation of relativistic self-focusing is now a well-developed tool capable, in principle, of replacing analytic theory. Nevertheless, despite the large number of published numerical results on relativistic self-focusing (e.g., [5,6,25–29,34]), they still cannot entirely compete with theory in terms of predictive capabilities because of the multiparametric nature of the problem. Moreover, numerical simulations cannot be regarded as an easy-to-use tool accessible to all in contrast to analytic formulas. Analytic theory can predict the behavior of self-focusing in the entire range of the controlling parameters. However, none of the analytic methods are able to provide an exact solution to the nonlinear Schrödinger equation (NLSE) for arbitrary boundary conditions. Only some specific boundary value problems that are far from practical applications have been solved so far. At the same time, numerical simulations in their concrete implementations can go beyond theoretical approaches by using more complicated plasma models, which are often closer to experimental conditions. Therefore, even an approximate analytic theory for practical boundary conditions being tested in simulations may advance the understanding of possible regimes of relativistic self-focusing. Both simulations and experiments demonstrate that relativistic self-focusing is accompanied by several characteristic effects, such as stationary and nonstationary channeling of a light beam, the formation of ring structures or numerous filaments [5,6,26,27,29,35], electron cavitation [28,36], and self-induced transparency [36–38]. We demonstrate that our theory reproduces some of these features.

As in [30], we here start from the reduced wave equation for a stationary circular-polarized light in a paraxial approximation for a medium with relativistic nonlinearity including the relativistic electron mass increase and the charge-displacement nonlinearity. Such a model based on the nonlinear Schrödinger equation is widely used to study propagation of electromagnetic wave beams in a plasma [6,29,36]. The physical picture of beam self-focusing in this model depends on the competition of two dimensionless parameters. One parameter describes the relative strength of the diffraction with respect to the relativistic electron mass nonlinearity, and the other is the laser intensity in the relativistic units and characterizes the contribution of the charge-displacement nonlinearity. As in the case of a medium with a cubic nonlinearity [30], the Cauchy problem is posed with a Gaussian radial distribution of the beam intensity at the entrance of the medium to find an approximate analytic NLSE solution and classify the possible self-focusing regimes describing this solution and depending on the controlling parameters.

The paper is divided into four sections and an Appendix. In Sec. II, we formulate the initial equations for the theoretical analysis of light beam propagation in a plasma with a relativistic nonlinearity, reducing the original NLSE to a pair of equations for the eikonal derivative and the electric field amplitude of the laser beam. In Sec. III, we obtain an approximate analytic solution of the derived equations using the renormalization-group symmetry method [30,33] (the details of the method are presented in the Appendix). We analyze our NLSE solution for a Gaussian beam at the plasma boundary. In the plane of controlling parameters, we analytically find the boundaries of the domains corresponding to different types of beam behavior, which is the result from our theory most important for experiments. In Sec. IV, we present examples of the spatial distributions of the electric field and electron density for different laser beam and plasma parameters. In Sec. V, we summarize and discuss the results.

II. BASIC EQUATIONS

To analyze the effects of the self-action of a light beam of relativistic intensity in a plasma, we start from the widely used mathematical model (see, e.g., [6] and Secs. 6 and 6.4.1 in [25]) in the form of the NLSE

$$2ik\partial_z E + \triangle_\perp E + k^2 \frac{\epsilon_{\rm nl}}{\epsilon_0} E = 0, \qquad E(0, \mathbf{r}) = E_0(\mathbf{r}), \quad (1)$$

for the complex electric field amplitude $E(z, \mathbf{r})$ of a circularly polarized electromagnetic wave (for the case of linear polarization the anisotropic effects can be important [39]) with the frequency ω slowly varying in the propagation direction z. Equation (1) corresponds to a paraxial (quasioptical) approximation describing the stationary structure of the wave beam. Here, $k = (\omega/c)\sqrt{\epsilon_0}$ is the wave number of the electromagnetic wave, $\triangle_\perp$ is the Laplace operator in the plane $\mathbf{r}$ perpendicular to the beam axis, z, $\epsilon_0 = 1 - 4\pi e^2 n_{e0}/(m_0\omega^2)$ is the linear dielectric permittivity of the plasma, and $\epsilon_{\rm nl}$ is the real part of the nonlinear permittivity of the plasma.

The nonlinearity in NLSE (1) is determined by the nonlinear refraction of the light beam given by the function $\epsilon_{\rm nl}$:

$$\epsilon_{\rm nl} = \epsilon_0 \frac{k_p^2}{k^2}\left(1 - \frac{n_e}{\gamma n_{e0}}\right), \qquad k_p^2 = \frac{4\pi e^2 n_{e0}}{m_0 c^2}. \quad (2)$$

It is due to two factors: (1) the relativistic nonlinearity of the electron mass, determined by the value of the relativistic factor $\gamma = \sqrt{1 + |E/E_{\rm rel}|^2}$, where $E_{\rm rel}^2 = (\omega c m_0/e)^2$, and (2) the charge-displacement nonlinearity, which determines the nonlinear deformation of the electron density $n_e = n_{e0} N_e(\gamma)$, proportional to $\triangle_\perp \gamma$. Usually, the well-known standard formula

$$N_e = \max\left\{0, 1 + k_p^{-2}\triangle_\perp \gamma\right\} \quad (3)$$

is used for N_e, which we follow also taking the standard condition of the non-negativity of the electron density $n_e \geqslant 0$ into

account, which allows describing a strong density modulation including the electron cavitation effect [6]. The modification of the piecewise smooth function (3) to obtain a smoothed transition from a vanishingly low electron density $N_e \to 0$ to a linear dependence on $\triangle_\perp \gamma$ by taking a weak thermal motion of electrons into account was discussed in [28,36]. As a possible example of such a modification, we can also use the smooth approximation

$$N_e = \frac{1 + k_p^{-2}\triangle_\perp \gamma}{1 - \exp\left[-\alpha_0\left(1 + k_p^{-2}\triangle_\perp \gamma\right)\right]}, \tag{4}$$

where the value of the positive parameter $\alpha_0 \gg 1$ determines the transition from the linear dependence of $N_e \propto \triangle_\perp \gamma$ to the exponentially decreasing $N_e \to 0$ with the intensity gradient change. Relying on arguments akin to those used in [28], we believe that there is no need for a concrete identification of the mechanism responsible for α_0 if the results for different $\alpha_0 \gg 1$ differ very little.

Using quasioptical approximation (1) establishes the applicability conditions for our theory, which is determined by the following constraints on the characteristic longitudinal and transverse scales $\Lambda_\parallel$ and $\Lambda_\perp$ of the complex amplitude E (also see [25]):

$$k\Lambda_\parallel, k_p\Lambda_\parallel \gg 1, \qquad k\Lambda_\perp^2 \approx \Lambda_\parallel \max\left\{1; (k\Lambda_\perp)^2 \frac{\epsilon_{\rm nl}}{\epsilon_0}\right\}. \tag{5}$$

The inequality in Eq. (5) means that the laser pulse length substantially exceeds the wavelengths of the corresponding electromagnetic and plasma fields. It allows neglecting the contribution of the term with the second derivative of the electric field with respect to the longitudinal coordinate z (along the beam axis) compared with the first term contribution to Eq. (1) when deriving the NLSE from more complicated equations. The approximate equality in Eq. (5) relates the characteristic transverse and longitudinal scales of the electric field caused by diffraction and nonlinearity. Using NLSE (1) involves considering only the electromagnetic wave propagating forward into the nonlinear medium and the absence of backward waves that could arise in the presence of sharp gradients of the dielectric constant of the medium in the longitudinal direction (see, e.g., p. 432 in Sec. 17.12 in [24]). Conditions (5) can be violated if the solution singularity appears where the characteristic longitudinal scale of the complex field amplitude sharply decreases. Hence, the analytic solution that we obtain characterizes the behavior of the beam in some finite spatial domain from the entrance up to the singularity point. This restriction follows from the mathematical model used based on the NLSE (also see the discussion of this question in Sec. 9.2 in [25]).

Using the standard representation for the complex field amplitude $E = A\exp(iks)$ and introducing $w \equiv A^2 = |E|^2$ and the derivative $\mathbf{v} = \{v, 0\} = \nabla_\perp s$ of the eikonal s along the radius, we reduce NLSE (1) to the two equations

$$\partial_z v + v\partial_r v - \frac{1}{2}\partial_r\left(\frac{1}{\sqrt{w}}(\triangle_\perp\sqrt{w}) + \rho^2 F\right) = 0,$$
$$\partial_z w + w\partial_r v + v\partial_r w + w\frac{v}{r} = 0,$$
$$F = 1 - \frac{N_e(\gamma)}{\gamma}, \quad \gamma = \sqrt{1 + i_0 w}. \tag{6}$$

In Eqs. (6), we use the following dimensionless variables for the coordinates and complex field amplitude:

$$z \to \sqrt{2\beta}\,\frac{z}{d}, \quad r \to \frac{r}{d}, \quad w \to \frac{w}{w_0}, \quad v \to \frac{v}{\sqrt{2\beta}}, \tag{7}$$

where $\beta = 1/2k^2d^2$, d is the characteristic transverse dimension of the light beam, and w_0 is the maximum value of w at the boundary of the medium. The contributions proportional to $\rho^2 = \omega_{\rm pe}^2 d^2/c^2$ and $i_0 = (e/\omega m_0 c)^2 w_0$ determine the role of the effects of the relativistic and charge-displacement nonlinearity given by the function F. The parameter i_0 can be written as the ratio of the maximum beam intensity $I_0 = (c/4\pi)w_0$ to the characteristic relativistic intensity $I_r = \omega^2 m_0^2 c^3/(4\pi e^2)$, i.e., $i_0 = I_0/I_r$. In the limit $i_0 w \ll 1$, the function F corresponds to a medium with cubic nonlinearity $\lim_{i_0 w\to 0} F = F_{\rm cub} = (i_0/2)w$.

Equations (6) should be supplemented by the boundary conditions that determine the structure of the beam at the entrance $z = 0$ of the nonlinear medium. Following, we consider a cylindrically symmetric beam with a plane initial phase front, i.e., with the zero eikonal derivative $v(0, r) = 0$ and a smooth distribution function for the square of the modulus of the electric field $w(0, r) \equiv J(r)$.

III. APPROXIMATE ANALYTIC SOLUTION: PROPAGATION OF A GAUSSIAN BEAM IN A PLASMA

To obtain an analytic solution of Eqs. (6), we use the method of renormalization-group symmetries [32]. This method consists in finding symmetries of a special kind that leave the approximate perturbative solution of Eqs. (6) (which holds at small distances from the boundary $z = 0$ of the nonlinear medium) invariant and using these symmetries to extend the approximate solution to the domain far from the boundary. We previously used this procedure to derive solution of Eqs. (6) in a medium with cubic and saturating nonlinearities [30,31]. More details on the implementation of this procedure for a medium with a relativistic nonlinearity are described in the Appendix. The resulting approximate analytic solutions for Eqs. (6) have the forms

$$v(z, r) = (z/2)\partial_\chi S, \quad w(z, r) = J(\mu)\frac{\chi}{r}\frac{\partial_{\chi^2} S}{\partial_{\mu^2} S}. \tag{8}$$

Here, the variables χ and μ are defined in terms of z and r using the relations

$$r = \chi(1 + z^2\partial_{\chi^2} S), \quad S(\mu) = S(\chi) + \frac{z^2}{4}(\partial_\chi S)^2 \tag{9}$$

with the function S depending on $\chi = r - vz$:

$$S(\chi) = \rho^2 F(J) + \frac{1}{\chi\sqrt{J(\chi)}}\partial_\chi[\chi\partial_\chi(\sqrt{J(\chi)})],$$
$$F(J) = 1 - \frac{N_e\{\gamma[J(\chi)]\}}{\gamma[J(\chi)]}, \tag{10}$$

and accounting for the effects of the relativistic and charge-displacement nonlinearity of the medium.

In the case where the nonlinear and diffraction contributions to (10) balance each other, i.e., for $S = 0$, we obtain a solution depending only on the coordinate r in the form of a waveguide configuration [30,31]. This occurs only for

certain forms of the distribution of the light beam electric field amplitude at the medium boundary. In the more general case, where the nonlinear and diffraction contributions do not balance each other [an arbitrary distribution of $J(r)$ at the entry into the medium], the electric field distribution in the medium is described by a two-dimensional solution (8) of system (6), depending on both r and z.

We note that in obtaining formulas of type (8) for the cubic nonlinearity or nonlinearity with saturation in [30,31], we made no initial assumptions concerning the spatial structure of the beam in the medium. Therefore, the relations obtained there are applicable for beams with arbitrary smooth boundary distributions. This is a fundamental difference from the case of relativistic nonlinearity under consideration because we must restrict the laser beam form at the entrance by requiring the absence of complete cavitation of electrons (we do not discuss the effect of cavitation of electrons at the boundary of the medium here). If this restraint is satisfied, then the only limitation that makes relations (8) approximate and not exact is due to the algorithm for deriving an approximate solution using approximate renormalization-group symmetries (see [30,31] and the Appendix for more details). Therefore, the correctness of the solution given by Eq. (8) depends on the validity of the already used quasioptical approximation (5) and the absence of explosionlike distortion of the spatial profile of the beam. Our renormalization-group algorithm, in principle, allows for the latter to occur, for example, as a result of breaking the profile $v(z, r)$. This is manifested in the characteristic propagation length $z_{\rm nl} \gtrsim \Lambda_{\rm nl}$, where $\Lambda_{\rm nl} = (\rho^2 F)^{-1}$ is determined by the considerable change in the beam intensity along its axis due to nonlinearity. Roughly speaking, the developed theory based on approximate renormalization-group symmetries is applicable for propagation distances before the solution singularity appears.

We emphasize that the solution Eqs. (8)–(10) of Eq. (6) are valid for arbitrary smooth function $N_e(\gamma)$ and therefore for the function (4) of interest. Correspondingly, the relations and plots depending on $N_e(\gamma)$, which are obtained below, use Eq. (4) with $\alpha_0 \gg 1$, where the dependence on α_0 is negligible.

Using Eqs. (8), we analyze the evolution of the laser beam with the initial Gaussian profile $J(r) = \exp(-r^2)$ and assume that the effect of electron cavitation does not appear at the boundary of the nonlinear medium. We can then even use in Eq. (10) the simplest expression for N_e, Eq. (3), which is itself a smooth function and does not require smoothing approximation, Eq. (4). The function F in Eq. (10) is determined only by the initial distribution of the square of the amplitude of the electric field of the beam at $z = 0$. We rewrite the expression for $S(\chi)$ after introducing the variable $p = \exp(-\chi^2)$ in the form

$$S(p) = \rho^2\left(1 - \frac{1}{\sqrt{1+i_0 p}}\right) - \frac{2}{1+i_0 p} - \frac{\ln p}{(1+i_0 p)^2}. \quad (11)$$

We recall that the applicability of Eq. (11) is limited only by distributions of electron densities that correspond to the condition that there is no effect of electron cavitation at the boundary of the nonlinear medium $z = 0$, i.e., cavitation does not occur when the inequality

$$\rho \geqslant \rho_{\rm cav}, \quad \text{where} \quad \rho_{\rm cav}^2 = 2i_0(1+i_0)^{-1/2}, \quad (12)$$

is satisfied. A characteristic feature of the solution given by Eqs. (8), (9), and (11) is the possibility of the growth of distortions of the wavefront of the beam with the coordinate z, up to breaking the profile $v(z, r)$. This happens when a single-valued dependence of r on χ is violated, i.e., when two conditions are met: $\partial_{\chi\chi} r = 0$ and $\partial_\chi r = 0$. The first condition defines the radial coordinate of the breaking point $r_{\rm br} = \sqrt{\ln 1/p_{\rm br}}(1 - z_{\rm br}^2\{p\partial_p S\}_{|p=p_{\rm br}})$ written in terms of $p_{\rm br}$, and the second gives the corresponding coordinate $z_{\rm br}$ along the beam axis. In the variables $\{z, p\}$, the conditions for the appearance of the solution singularity can be written as

$$\left\{p\sqrt{\ln\frac{1}{p}}[3(\partial_p S + p\partial_{pp}S) + 2\ln p(\partial_p S + 3p\,\partial_{pp}S + p^2\partial_{ppp}S)]\right\}_{|p=p_{\rm br}} = 0, \quad (13)$$

$$z_{\rm br}^2 = \{[p\,\partial_p S + 2\ln p(p\,\partial_p S + p^2\partial_{pp}S)]^{-1}\}_{|p=p_{\rm br}}. \quad (14)$$

Solutions of the equation for $p_{\rm br}$ in Eq. (14) correspond to either of its two factors vanishing, i.e., either (a) $\ln(1/p_{\rm br}) = 0$, which corresponds to the appearance of the axial singularity $p_{\rm br} = 1$, or (b) the expression in square brackets in Eq. (14) vanishes, which corresponds to the off-axis singularity $p_{\rm br} \neq 0$. We analyze these two cases separately.

(a) *The appearance of the axial singularity* $p_{\rm br} = 1$. The simplest form of Eqs. (14) is obtained at $p_{\rm br} = 1$, when a singularity appears on the beam axis at the point $\{z_{br}\}_{p=1} \equiv z_{\rm axis}$ defined by the equality

$$z_{\rm axis}^2 = \left[\frac{\rho^2 i_0}{2}\frac{1}{(1+i_0)^{3/2}} + \frac{2i_0 - 1}{(1+i_0)^2}\right]^{-1}. \quad (15)$$

The positivity condition $z_{\rm axis}^2 > 0$ determines the range of parameters ρ^2 and i_0 for which there exists an axial singularity

$$\rho > \rho_{\rm axis}, \quad \text{where} \quad \rho_{\rm axis}^2 = \frac{2}{i_0}(1-2i_0)(1+i_0)^{-1/2}, \quad i_0 \leqslant \sqrt{2} - 1. \quad (16)$$

The minimum beam radius $\rho_{\rm axis}$ depending on i_0 above which an axial singularity appears corresponds to the limit $z_{\rm axis}^2 \to \infty$ in (15). The upper limit of i_0 in Eq. (16) is given by the condition of the absence of the electron cavitation effect at $z = 0$ and corresponds to $\rho_{\rm axis} \geqslant \rho_{\rm cav}$. For a higher laser beam intensity $i_0 > \sqrt{2} - 1$, the allowable range of the beam radius is cut from the side of small values by the condition $\rho > \rho_{\rm cav}$.

(b) *The appearance of an off-axis singularity* $p_{\rm br} \neq 1$. The off-axis singularity corresponds to a nonzero value $p_{\rm br} \neq 1$ given by the condition $\partial_{\chi\chi} r = 0$, which in this case becomes

$$[3(\partial_p S + p\,\partial_{pp}S) + 2\ln p(\partial_p S + 3p\,\partial_{pp}S + p^2\partial_{ppp}S)]_{|p=p_{\rm br}} = 0. \quad (17)$$

The boundary of the domain of parameters for which there exists an off-axis singularity is determined by the equation

$$\rho = \rho_{\rm off}, \quad \text{where} \quad \rho_{\rm off}^2 = \frac{8(3-i_0)}{(i_0-2)\sqrt{1+i_0}} \quad (18)$$

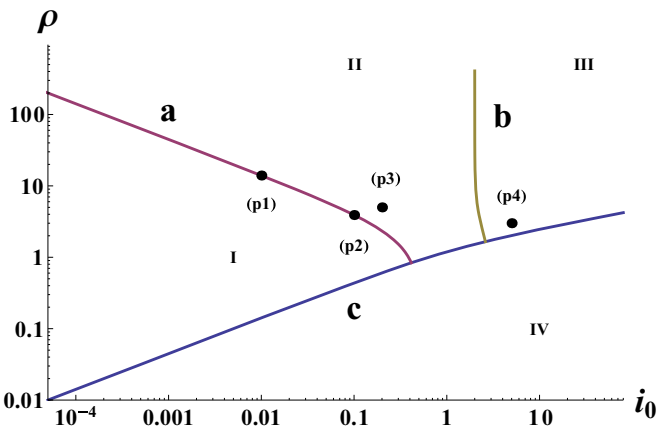

FIG. 1. The boundaries of the domains I, II, III, and IV on the parameter plane $\{i_0, \rho\}$ for different types of solutions (8). These boundaries are defined by the relations $\rho = \rho_{\text{axis}}(i_0)$ (curve a, boundary between I and II), $\rho = \rho_{\text{off}}(i_0)$ (curve b, boundary between II and III), and $\rho = \rho_{\text{cav}}(i_0)$ (curve c, boundary between IV and all the others, I, II, and III).

for $2 < i_0 \leqslant \sqrt{13} - 1$. For greater beam intensity values $i_0 > \sqrt{13} - 1$, the lower boundary of the beam radius is given, as in case (a), by the condition $\rho > \rho_{\text{cav}}$. Comparing Eqs. (16) and (18) shows that the boundary of the domain for the solution with the off-axis singularity is at greater beam intensities than the domain for the solution with the axial singularity.

Combining the above conditions on the beam-plasma parameters given by Eqs. (12), (16), and (18), we obtain the partitioning of the controlling parameter plane into several domains. A graphical representation on the parameter plane $\{i_0, \rho\}$ in terms of the domain boundaries is shown in Fig. 1. The domains are labeled by the numbers I, II, III, and IV and characterize qualitatively different behaviors of the laser beam in plasma. The curves separating these domains are defined as follows. The boundary between the domains I and II (curve a) is defined by the equation $\rho = \rho_{\text{axis}}(i_0)$. The boundary between the domains II and III (curve b) is defined by the equation $\rho = \rho_{\text{off}}(i_0)$. The boundary between the domain IV and all the other domains (curve c) is defined by the equation $\rho = \rho_{\text{cav}}(i_0)$. Although the parameter plane describes the laser beam behavior in a wide range of parameters, extremely small values of ρ are excluded from our consideration by constraints (5) on the theory.

Knowing the boundaries of the domains in the parameter plane $\{\rho, i_0\}$ makes it much easier to analyze the type of solutions and the conditions for the appearance of the solution singularities. This is an important finding in the theory of relativistic self-focusing. Even if there is no solution singularity, i.e., in domain I, a specific regime for a light beam with relativistic nonlinearity still exists, which is of physical interest. Namely, this is the regime in which the intensity of the beam along the axis is preserved at distances exceeding the diffraction length defining divergence of light rays in a linear medium. Such a beam self-trapping mode occurs when its radius is close to ρ_{axis} given by (16) but does not exceed it; the point in the parameter domain is close to curve a.

For the plasma and beam parameters related to domains II and III, the appearance of the axial singularity, whose

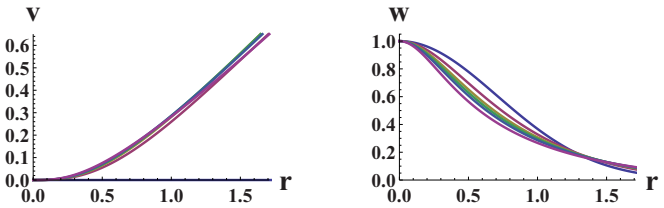

FIG. 2. The spatial distribution of the eikonal derivative v (left image) and the square of the amplitude of the electric field of the light beam w (right image) for different values of the longitudinal coordinate z along the beam axis for $i_0 = 0.01$ and $\rho = 13.96$: the different curves correspond to the transition from $z = 0$ to $0.6; 0.8; 0.9; 1.0; 1.2$. An increase of z is accompanied by a clearly discernible decrease of w in the region of small $r \to 0$.

coordinate is found from formula (15), is possible if the condition $\{p\,\partial_p S\}_{p=1} > 0$ is satisfied. Similarly, for plasma and beam parameters related to domain III, the condition for the appearance of an off-axis singularity can be satisfied. The corresponding "radial coordinate" p_{br} of the singularity for the given values of i_0 and ρ is found from Eq. (17) if the inequality $\{p\,\partial_p S + 2\,\ln p(p\,\partial_p S + p^2\partial_{pp} S)\}_{p=p_{\text{br}}} > 0$ is satisfied. If this condition is satisfied, then the coordinate of the singularity point along the beam axis z_{br} can be found from Eq. (14) using the previously found value p_{br}. In general, solution (8) can be characterized by several singularities with different longitudinal coordinates. Comparing these coordinates allows identifying the smallest of them, which characterizes the most rapidly manifested singularity. Beyond the point of this singularity, the obtained solution (8) becomes inapplicable, limiting the applicability domain of the theory. We do not discuss domain IV of parameters corresponding to the effect of cavitation of electrons at the boundary of the medium in this paper.

IV. EXAMPLES OF THE LASER FIELD AND ELECTRON DENSITY SPATIAL DISTRIBUTIONS

To illustrate the results obtained above, we now present plots of the spatial distributions of the eikonal derivative, the square of the amplitude of the light beam electric field, and the electron density obtained above using approximate analytic solution (8) for the four sets of parameters i_0 and ρ corresponding to the four points (p1), (p2), (p3), and (p4) in Fig. 1.

The first two examples correspond to those values of i_0 and ρ for which the points (p1) and (p2) in the plane $\{i_0, \rho\}$ are to the left of curve a but very close to it. In this case, the nonlinearity partially compensates the diffraction spreading of the beam as the z increases but not so much as to lead to the formation of a singularity. Such a regime in which the beam intensity in the near-axis region is preserved at distances exceeding the length at which the beam diffraction divergence occurs in a linear medium is called the self-trapping mode of the wave beam. This mode is illustrated in Figs. 2 and 3, where the spatial distribution of the eikonal derivative v and the square of the amplitude w of light beam electric field are shown for $i_0 = 0.01$, $\rho = 13.96$ [point (p1)] and for $i_0 = 0.1$, $\rho = 3.99$ [point (p2)] for different values of the coordinate z

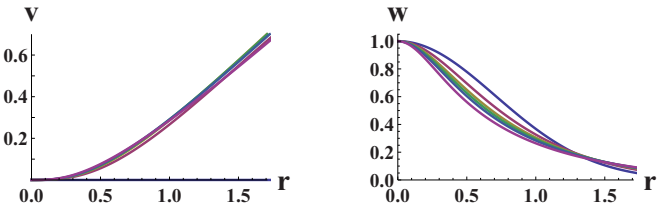

FIG. 3. The spatial distribution of the eikonal derivative v (left image) and the square of the amplitude w of the electric field of the light beam (right image) for different values of the longitudinal coordinate z along the beam axis for $i_0 = 0.1$ and $\rho = 3.99$: the different curves correspond to the transition from $z = 0$ to $0.6; 0.8; 0.9; 1.0; 1.2$. An increase of z is accompanied by a clearly discernible decrease of w in the region of small $r \to 0$.

along the beam axis. Comparing the plots in Figs. 2 and 3 shows their qualitative and quantitative similarity, and the difference is manifested in the plots of the spatial distribution of the electron density presented in Fig. 4. We note that for the parameters corresponding to points (p1) and (p2) in the plane $\{i_0, \rho\}$, the role of the ponderomotive charge-displacement is negligibly small, the electron density perturbations are very low, and there is no cavitation of electrons.

The next example corresponds to values of the parameters i_0 and ρ for which the point on the plane $\{i_0, \rho\}$ is in domain II, i.e., between curves a and b. As follows from the results obtained above, a solution singularity in this case can arise, developing on the beam axis. The illustration of this focusing on the axis regime is presented for the parameter values $i_0 = 0.2$ and $\rho = 5$ corresponding to point (p3) in Fig. 1. The plots of the spatial distributions of the eikonal derivative v and the square of the amplitude w of the electric field of the light beam for different values of the coordinate z are shown in Fig. 5.

Finally, the last example corresponds to values of the parameters i_0 and ρ for which the point on the plane $\{i_0, \rho\}$ is in domain III, i.e., to the right of curve b. In this case, there is a possibility to develop both off- and on-axis solution singularities, which for the parameter values $i_0 = 5$, $\rho = 3$ corresponding to point (p4) in Fig. 1 appear at $z_{\mathrm{br}} \approx 0.686$ (off-axis singularity) and at $z_{\mathrm{axis}} \approx 0.749$ (for the on-axis singularity). The plots of the spatial distributions of the eikonal derivative v and the square of the amplitude w of the electric field of the light beam for this example are shown for different values of the coordinate z in Fig. 6. Because the z_{axis} value exceeds z_{br}, the off-axis feature appears more explicitly in the form of a ring structure shown in Fig. 6, although the square

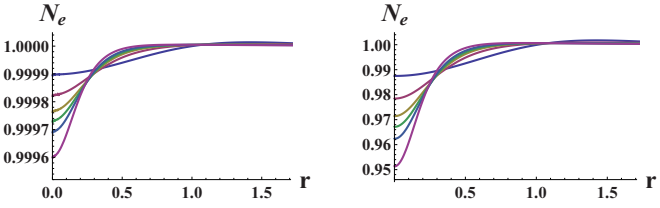

FIG. 4. The spatial distribution of the electron density N_e corresponding to the intensity distribution of the laser beam for the plasma and beam parameters in Figs. 2 (left image) and 3 (right image).

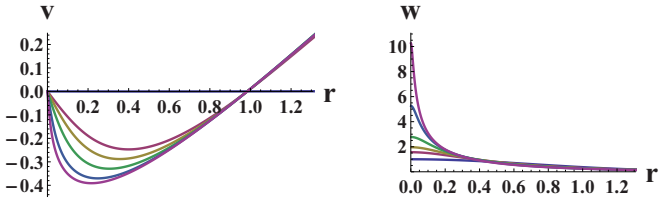

FIG. 5. The spatial distribution of the eikonal derivative v (left image) and the square of the amplitude w of the electric field of the light beam (right image) for different values of the longitudinal coordinate z along the beam axis for $i_0 = 0.2$ and $\rho = 5$: the value of the longitudinal coordinate of the axial singularity for the chosen parameter values $i_0 = 0.2$ and $\rho = 5$, given by condition (15), is equal to $z_{\mathrm{axis}} = 0.82$. The different curves correspond to the transition from $z = 0$ to $0.6z_{\mathrm{axis}}; 0.7z_{\mathrm{axis}}; 0.8z_{\mathrm{axis}}; 0.9z_{\mathrm{axis}}; 0.95z_{\mathrm{axis}}$ from the top down for curves in the left image and from the bottom up in the right image (for small $r \to 0$).

of the amplitude of the electric field on the beam axis also increases.

The form of the spatial distributions of $v(r)$ shown in Figs. 5 and 6 demonstrates the characteristic peculiarity of solutions (8), which was noted in [31]: these solutions correspond to a waveguide-type configuration of the light beam. Indeed, it follows from formulas (8) that the value of the radius r_{w} for which v vanishes is the same for all z for which the solution is given. Integrated over the radius in the range $0 \leqslant r \leqslant r_{\mathrm{w}}$ with the weight r, the square of the amplitude of the electric field of the beam $M_{\mathrm{w}} = \int_0^{r_{\mathrm{w}}} dr\, rw$ is conserved in the domain inside the radius r_{w} according to the second equation in (6). The redistribution of the amplitude inside this domain accompanying the change in the coordinate z does not change the fraction of the total energy inside the radius r_{w}. Therefore, such a structure of a light beam can be called the waveguide-type configuration with the waveguide radius r_{w}. The domain in the plane $\{i_0, \rho\}$ where the waveguide-type configurations are realized is located to the right of the curve given by the solution of the equation $\rho = \rho_{\mathrm{axis}}$.

For the distributions of $w(r)$ shown in Figs. 5 and 6, the spatial gradient of the amplitude of the light beam electric

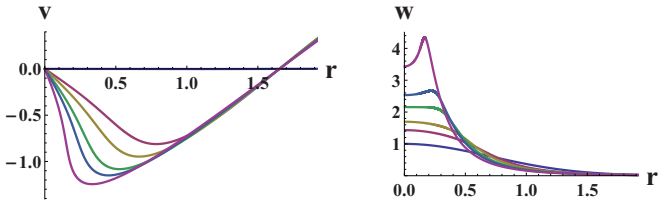

FIG. 6. The spatial distribution of the eikonal derivative v (left image) and the square of the amplitude w of the electric field of the light beam (right image) for different values of the longitudinal coordinate z along the beam axis for $i_0 = 5$ and $\rho = 3$: the values of the longitudinal coordinates of the on- and off-axis singularities for the chosen parameter values are $z_{\mathrm{axis}} \approx 0.564$ and $z_{\mathrm{br}} \approx 0.454$. The different curves correspond to the transition from $z = 0$ to $0.6z_{\mathrm{br}}; 0.7z_{\mathrm{br}}; 0.8z_{\mathrm{br}}; 0.85z_{\mathrm{br}}; 0.92z_{\mathrm{br}}$ from the top down for curves in the left image and from the bottom up in the right image (for small $r \to 0$).

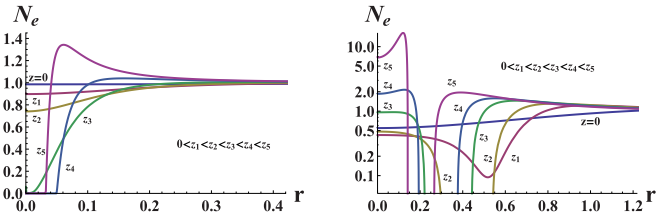

FIG. 7. The spatial distribution of the electron density N_e corresponding to the intensity distribution of the laser beam for the plasma and beam parameters in Figs. 5 (left image) and 6 (right image). The effect of electron cavitation in the axial zone in the left image and in the off-axis zone in the right image is clearly visible.

field increases along the distance from the boundary of the medium: near its axis for the on-axis singularity variant and in the zone of ring formation for the off-axis singularity variant. Therefore, we should expect manifestation of electron cavitation. Describing the electron density dynamics requires considering the conservation law for the total number of electrons and therefore presents certain difficulties in modeling the relativistic laser-plasma interaction numerically [6,28]. The approximate analytic approach used does not claim to describe the electron cavitation process exhaustively, but it gives the possibility of analyzing this phenomenon qualitatively with relation (4), which uses the intensity distribution (8) of the laser beam expressed it terms of its characteristics at the plasma boundary. More importantly, these results can be improved using the next-order approximation in the parameters involved in constructing the renormalization-group symmetry. As a confirmation of this, we show plots in Fig. 7 of the spatial distributions of the electron density for the propagation of a laser beam with parameters corresponding to Figs. 5 and 6. It can be seen that the steepening of the profile of the electric field leads to forming an area of electron cavitation either in the vicinity of the beam axis (in case of an on-axis singularity) or in the off-axis region (in case of an off-axis singularity), which correctly characterizes the electron cavitation process qualitatively.

We note that a result of type (8) can also be obtained in the case where complete cavitation of electrons already occurs at the plasma boundary, but such an analysis is beyond the scope of this paper.

V. DISCUSSION AND SUMMARY

To conclude, we emphasize that we have here reported analytic results for relativistic self-focusing in the NLSE model. For a laser beam in a plasma with relativistic and ponderomotive charge-displacement effects, we obtained an approximate analytic solution of the Cauchy problem as a series of several types of solutions. We analyzed the solutions to describe the channeled longitudinal-radial distribution of the light beam intensity in plasma with a Gaussian beam at the boundary. The technique used is based on the theory of transformation groups.

It is a common knowledge that methods of a classical group analysis allow one to derive exact solutions to the NLSE in 1D, 2D, and 3D geometries for cubic and quintic nonlinearities (see Refs. [40,41]). It is especially important for multidimensional solutions of the NLSE, which cannot be integrated by the inverse scattering method (see Ref. [42]). However, boundary conditions for the solutions just mentioned do not correspond to a localized electromagnetic beam at the entry plane. The key idea of our approach to the solution of the NLSE consists of finding a special class of symmetries for the chosen boundary value problem. It does not imply any *a priori* assumptions and provides an approximate analytical solution to a specific boundary value problem. The renormalization-group symmetry method has already been applied for the analysis of a number of particular solutions for NLSE for media with cubic and saturating nonlinearities [30,31]. In our paper [30], which used the renormalization-group symmetry approach to the NLSE with cubic nonlinearity, we have proven that the assumptions used about the profile of the incident beam, axial symmetry, and the type of a nonlinearity are not restrictive. We believe that renormalization-group symmetry approach for relativistic media will work well for the problems of higher dimensionality to describe, e.g., beam filamentation, multifocus structure formation, etc., in the case of arbitrary smooth light beams at the plasma entry.

A consequence of the approximate analytic approach is the appearance of a singularity in the self-focusing solution: wave breaking of the profile of the beam eikonal derivative with respect to the radius occurs at a finite coordinate along the beam axis and hence limits the applicability of the theory. The analytic theory hence describes self-focusing at a limited distance from the boundary of the medium and does not pretend to describe the behavior of the beam far from it, where the applicability conditions for the theory are violated and multifocus structures, bundle of rays, etc., can be formed. Despite the limitations of the theory associated with using approximate transformation groups, it explicitly gives the dependence of the solutions on the controlling parameters such as the dimensionless characteristic beam radius $\rho = \omega_{\rm pe} d/c$ and the ratio $i_0 = I_0/I_r$ of the maximum beam intensity to the characteristic relativistic value. This advantageously distinguishes the obtained analytic solutions from the results of numerical simulations and allows predicting the properties of self-focused beams in a wide range of laser-plasma parameters and the behavior of the laser beam under given experimental conditions. In turn, the variety of experimental conditions in which relativistic self-focusing can manifest itself is dictated by the wide range of applications of modern laser beams with a relativistic intensity.

Describing laser beam propagation in an extended plasma is very important for realizing fast ignition in laser fusion [17], for obtaining high-energy electrons (e.g., in the wake field excitation regime [12]), and for ensuring the penetration of laser radiation through preplasma in front of an irradiated target [18]. In dimension variables, the radius of the beam and its intensity at the boundary of the medium are expressed in terms of the parameters ρ and i_0, the ratio $\omega/\omega_{\rm pe}$, and the wavelength of the laser λ as

$$d \approx 0.16 \frac{\omega}{\omega_{\rm pe}} \lambda[\mu\text{m}]\, \rho \quad (\mu\text{m}),$$

$$I_0 \approx 2.74 \times 10^{18} \left(\frac{1}{\lambda[\mu\text{m}]} \right)^2 i_0 \quad (\text{W/cm}^2). \qquad (19)$$

The character of the spatial redistribution of the beam energy depends on the initial beam radius and the beam intensity. Knowing the boundaries of different parameter domains can greatly facilitate and supplement numerical experiments in a detailed investigation of specific regimes of the laser beam evolution. We have analytically determined the conditions for the appearance of various beam self-focusing regimes, leading either to the appearance of an axial singularity in the distribution of the square of the amplitude of the electric field of the beam (focusing on the axis) or to the appearance of maximums of the electric field at a finite value of the radius outside the beam axis (off-axis feature). In addition, the plasma-beam parameters are specified for the regime of a propagation of a relativistic laser beam in which a singularity does not arise but the square of the amplitude of the electric field of the beam on the axis practically does not decrease at distances comparable to the diffraction length. This was demonstrated with four examples of typical laser-plasma channels defined by points (p1), (p2), (p3), and (p4) in Fig. 1.

For a low beam intensity i_0 and for a beam radius close to but not exceeding the value ρ_{axis}, beam propagation occurs in a self-capture mode, which was demonstrated for the parameters corresponding to points (p1) and (p2). A similar regime was observed in [43,44] for one-dimensional or almost one-dimensional solutions of the NLSE model with an amplitude A that is constant or varies slowly with the coordinate z in the paraxial approximation [44] and in [43] from the analysis of beam propagation with a transverse electric field shape close to the lowest eigenmode of the stationary NLSE solution. For a moderate beam intensity, comparable to the relativistic value I_r in order of magnitude, and for a large radius $\rho \gg \rho_{\text{axis}}$, the "classical" mode of self-focusing on the axis is realized [variant (p3)]. An overwhelming number of works on numerical simulation of relativistic self-focusing demonstrate this best-known regime [5,6,25,29]. Finally, an intensity significantly exceeding the relativistic intensity value leads to the formation of a transverse ring structure (tube beam) as the light beam propagates deep into the medium [variant (p4)]. Such a regime was observed in numerical simulations [25], [p. 142], but in contrast to the example we considered, it corresponded to a ring-type channel with an intensity in the ring zone lower than in the accompanying central filament. Another version of the ring structure, closer to the one shown in Fig. 6 and in which the electric field intensity in the ring zone exceeds the intensity at the beam axis, was observed in particle-in-cell (PIC) simulations for $n_{e0}/n_{cr} < 0.1$ [27,34]. For significantly higher electron density $n_{e0}/n_{cr} = 0.36$, the channel structure, which corresponds to a ring and a central filament, was observed in Ref. [45]. Meanwhile, Ref. [27] reports that ring structure is not stable against azimuthal perturbations for dense plasma. Stability analysis of the channel solutions, which appear in our theory, is beyond the scope of this paper. However, it is obvious that future studies should address this issue.

We note that according to Eqs. (19) for the different beam modes shown in Figs. 2, 3, 5, and 6, the maximum intensity of laser radiation at the medium boundary is $I_0(\lambda[\mu\text{m}])^2 = 0.027 \times 10^{18}$ W/cm^2 for variant (p1), $I_0(\lambda[\mu\text{m}])^2 = 0.274 \times 10^{18}$ W/cm^2 for variant (p2), $I_0(\lambda[\mu\text{m}])^2 = 0.548 \times 10^{18}$ W/cm^2 for variant (p3), and $I_0(\lambda[\mu\text{m}])^2 = 13.7 \times 10^{18}$ W/cm^2 for variant (p4). These values are typical for experiments and numerical calculations on relativistic self-focusing [5,6,25,27,29,34].

Historically, the theoretical models of relativistic self-focusing were developed aimed primarily at establishing the so-called critical power, above which the beam becomes self-focused as a result of the predominance of nonlinearity over diffraction. Up to now, most papers dealing with relativistic self-focusing refer to the value $P_c \approx 17(\omega^2/\omega_{\text{pe}}^2)$ GW as a critical power. However, it has already been observed in the simulations [43] that self-focusing regimes may occur at the beam powers less than P_c. Following, we explain in details how this happens.

The critical power $P_c \approx 17(\omega^2/\omega_{\text{pe}}^2)$ GW was obtained from a one-dimensional solution of the NLSE as a threshold value of the beam power above which relativistic self-focusing arises [5]. In our study here, we analyzed two-dimensional NLSE solutions with singularities that arise both on the beam axis and outside the axis (ring structure) and also solutions characterizing beam self-trapping. The power of a Gaussian beam at the entrance to the medium, which characterizes such solutions, can be either larger or smaller than P_c. If we formally rewrite the given power of a Gaussian beam at the plasma boundary as a function of the used dimensionless beam and plasma parameters,

$$P = \frac{\rho^2 i_0}{4}\frac{\omega^2}{\omega_{\text{pe}}^2}\frac{m^2c^5}{e^2} \approx 2.18\,\frac{\omega^2}{\omega_{\text{pe}}^2}\rho^2 i_0\ (\text{GW}), \qquad (20)$$

in accordance with Fig. 1, we then have $\rho^2 i_0 = 1.95$ for variant (p1), $\rho^2 i_0 = 1.525$ for variant (p2), $\rho^2 i_0 = 5$ for variant (p3), and $\rho^2 i_0 = 45$ for variant (p4). Estimates of the beam powers for these regimes correspondingly yield $P_{\text{p1}} \approx 4.251(\omega^2/\omega_{\text{pe}}^2)$ GW, $P_{\text{p2}} \approx 3.325(\omega^2/\omega_{\text{pe}}^2)$ GW, $P_{\text{p3}} \approx 10.9(\omega^2/\omega_{\text{pe}}^2)$ GW, and $P_{\text{p4}} \approx 98.1(\omega^2/\omega_{\text{pe}}^2)$ GW. All these regimes correspond to laser beam nonlinear channeling, and the lowest power corresponds to variant (p2). At the same time, the largest power is for variant (p4). Self-trapping regimes of variants (p1) and (p2) with the lowest power corresponding to the condition where the diffraction beam divergence is balanced by the relativistic nonlinearity are physically most appropriate to be called the critical laser power. The minimum value of the power for the Gaussian beam at the boundary of the medium for such a regime follows from Eq. (20) at $i_0 = \sqrt{2} - 1$ in view of Eq. (16) and is equal to $P_{\text{min}} \approx 0.629(\omega^2/\omega_{\text{pe}}^2)$ GW. This value is significantly smaller than the commonly used value of P_c. The relative excess of P_{p1}, P_{p2}, P_{p3}, and P_{p4} over the minimal power P_{min} is 6.76 for variant (p1), 5.29 for variant (p2), 17.33 for variant (p3), and 155.96 for variant (p4). These estimates qualitatively agree with the results of the numerical experiment [27] in which the formation of a ring structure in a plasma was observed only with a relativistic laser beam power significantly exceeding (more than 30 times) the critical value. We note that the power values of the beams propagating in a plasma with the above discussed parameters shown in Fig. 1 and for characteristic values of the plasma density $n_{e0}/n_{cr} = (\omega_{\text{pe}}/\omega)^2$ from 0.005 to 0.1 are in the range from 0.1 to 600 TW, which is currently being intensively used in numerical simulations [6,25,27] and in experiments [25,46,47].

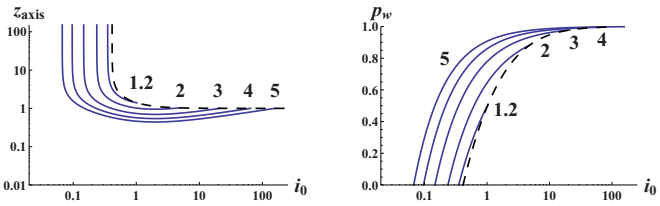

FIG. 8. The dependencies of $z_{\rm axis}$ (left image) and $p_{\rm w}$ (right image) on i_0 for different $\rho = 5, 4, 3, 2$, and 1.2. The dashed curves in both images limit the range of i_0 for each given ρ due to the condition of no initial cavitation $\rho_{\rm cav} = \rho$.

Aside from the parameters ρ and i_0, which define different regimes of beam self-focusing, there are two additional characteristics for the domains II and III, the distance to the singularity $z_{\rm br}$ or $z_{\rm axis}$, defined by Eqs. (14) and (15) and fraction of the beam power inside the waveguide with the radius $r_{\rm w}$, defined as $p_{\rm w} \equiv P_{\rm w}/P = 1 - p(r_{\rm w})$. The knowledge of these parameters helps to better understand relation between the distance at which the singularity occurs and the fraction of the beam power trapped within. To illustrate this point, the plots for the dependencies $z_{\rm axis}(i_0)$ (left image) and $p_{\rm w}(i_0)$ (right image) at different values of ρ are shown in Fig. 8. For any given value of ρ, each of the curves in Fig. 8 (both $z_{\rm axis}$ and $p_{\rm w}$) ends at some cutoff intensity $i_{\rm max}$,

$$i_{\rm max} = \rho^4/8 + (\rho^2/2)\sqrt{1+\rho^4/16}\,, \tag{21}$$

when electron cavitation occurs, $\rho_{cav} = \rho$. For $2^{3/8}(\sqrt{2}-1)^{1/2} < \rho < 2/3^{1/4}$ the value of $z_{\rm axis}$ steadily decreases with i_0, while for $\rho > 2/3^{1/4}$ each curve $z_{\rm axis}(\rho, i_0)$ reaches the minimum $z_{\rm axis}(\rho, 2) = \sqrt{3}(1+\rho^2/\sqrt{3})^{-1/2}$ at $i_0 = 2$.

It is of interest to compare our dependencies described by the curves on Figs. 1 and 8 with those from a conception of eigenmodes for NLSE (see, e.g., [6,25]). These one-dimensional modes, depending only on the transverse coordinate r, can be obtained from the first equation in Eq. (6) where the first two terms proportional to $\partial_z v$ and $\partial_r v$ are omitted. Formally, this also follows from the equation $S(J) =$ const, where $S(J)$ is defined by Eqs. (10) and $J = J(r)$. One might expect the similar relation between ρ and i_0 for the base eigenmodes of NLSE and the Gaussian beam with $z_{\rm axis} \to \infty$. As an illustration, consider the self-trapping regime. In the often discussed case of $N_e = 1$ when charge-displacement nonlinearity is omitted we get $S_{\rm nocav} = \rho^2(1 - 1/\sqrt{1+i_0 p}) - 2 - \ln p$ and the following expression for the singularity coordinate $z_{\rm nocav} = ((\rho^2 i_0/2)(1+i_0)^{-3/2} - 1)^{-1/2}$. In the limit $z_{\rm nocav} \to \infty$, we get $\rho_{\rm nocav} = \sqrt{2/i_0}(1+i_0)^{3/4}$. This relation corresponds to the result suggested in Ref. [44] as the self-trapping condition. In accordance with Eq. (20), the light beam power of the least radius $\rho_{\rm nocav,min} = 3^{3/4}$, which is achieved at $i_0 = 2$ is given by $P_{\rm nocav}(i_0 = 2) \approx 22.66(\omega^2/\omega_{\rm pe}^2)$ GW. The estimate obtained is comparable to the generally accepted value of the critical power P_c, i.e., order of magnitude higher than the above discussed value $P_{\rm min}$. This demonstrates that the critical power for relativistic self-focusing depends not only on the beam intensity distribution at the plasma entrance, but also on a concrete model of nonlinearity.

When written in dimensional variables, the distance from the plasma boundary to the point $z_{\rm br}$ of the solution singularity reads as

$$L_{\rm sing} \approx 0.16\left(\frac{\omega}{\omega_{\rm pe}}\right)^2 \rho^2 \lambda[\mu{\rm m}]\, z_{\rm br}\ (\mu{\rm m}). \tag{22}$$

For the parameters in Figs. 5 and 6, this formula for $n_{e0}/n_{cr} = 0.036$ and $\lambda = 1\ \mu$m gives 91.1 μm for Fig. 5 (axial singularity) and 90.8 μm for Fig. 6 (off-axis singularity). These values show an order-of-magnitude agreement with the results of the numerical experiment [27], where similar solutions with either an on-axis peak or a ring electric field structure were obtained. We note that formula (22) corresponds to the upper limit for our theory: we cannot apply our results for $z > z_{\rm br}$, while numerical experiments produce results beyond this point. Hence, comparing numerical results with our analytic results is reasonable if we consider beam self-focusing for $z < z_{\rm br}$.

ACKNOWLEDGMENT

This work was supported by the Russian Science Foundation, Grant No. 17-12-01283. The employed mathematical procedure presented in Appendix was developed with partial support of the Russian Foundation for Basic Research, Grant No. 18-01-00890.

APPENDIX: APPROXIMATE SOLUTION OF NLSE (6) WITH RELATIVISTIC NONLINEARITY BY THE RENORMALIZATION-GROUP SYMMETRY METHOD

We here describe the construction of approximate solutions of NLSE (6) with relativistic nonlinearity using the method of renormalization-group symmetries [32]. This method consists in finding symmetries of a special kind under which approximate solutions of (6) constructed by perturbation theory for small distances from the boundary of a nonlinear medium are invariant and then applying these symmetries to extend the approximate solutions to the bulk of the nonlinear medium. Such a procedure is based on the property of a renormalization-group symmetry operator to transform a solution of a boundary value problem with given boundary data into a solution of the same boundary value problem. To construct the renormalization-group symmetry operator, following the general renormalization-group symmetry algorithm [30,32], we use the Lie-Bäcklund symmetries admitted by the original differential equations (6) and determined by the canonical group operator

$$X = f\,\partial_v + g\,\partial_w. \tag{A1}$$

The coordinates f and g of this operator are found by solving the corresponding determining equations expressing the invariance conditions for system (6) with respect to the group with operator (A1):

$$\begin{aligned} &D_z f + v D_r f + f v_1 - \partial_w(B) g - \partial_{w_1}(B) D_r g \\ &\quad - \partial_{w_2}(B) D_r^2 g - \partial_{w_3}(B) D_r^3 g = 0, \\ &D_z g + w D_r f + v D_r g + g v_1 + f w_1 + \frac{vg}{r} + \frac{fw}{r} = 0. \end{aligned} \tag{A2}$$

Here,

$$B = \frac{1}{2}D_r\left(\frac{D_r(rD_r\sqrt{w})}{r\sqrt{w}}\right) + \frac{1}{2}D_r(\rho^2 F),$$
$$v_s \equiv \frac{\partial^s v}{\partial r^s}, \quad w_s \equiv \frac{\partial^s w}{\partial r^s}, \tag{A3}$$
$$D_r = \partial_r + \sum_{s=0}^{\infty}(v_{s+1}\partial_{v_s} + w_{s+1}\partial_{w_s}),$$

and D_z is represented as $D_z = D_z^0 + D_z^1$, where

$$D_z^0 = \partial_z - \sum_{s=0}^{\infty}\left\{D_r^s(vv_1)\partial_{v_s} + \left[D_r^{s+1}(wv) + D_r^s\left(\frac{wv}{r}\right)\right]\partial_{w_s}\right\},$$
$$D_z^1 = \sum_{s=0}^{\infty} D_r^s(B)\partial_{v_s}. \tag{A4}$$

Because the terms originating from B in the first equation in (6) in the case of a slowly varying electric field amplitude are considered small compared with the first and the second terms, we seek f and g in the form of a series expansion in powers of the "dimensionless relative amplitude" b of the contributions from B:

$$f = \sum_{i=0}^{\infty} f^i, \qquad g = \sum_{i=0}^{\infty} g^i. \tag{A5}$$

We restrict ourselves to only the first-order corrections

$$f = f^0 + f^1 + o(b), \qquad g = g^0 + g^1 + o(b), \tag{A6}$$

where $f^0 \propto O(1)$, $g^0 \propto O(1)$, $f^1 \propto O(b)$, and $g^1 \propto O(b)$. We substitute (A6) in the determining Eqs. (A2) and collect the zeroth- and first-order terms, obtaining

$$M_0 f^0 = 0, \qquad M_1 g^0 + M_2 f^0 = 0,$$
$$M_0 f^1 + D_z^1 f^0 - \partial_w(B)g^0 - \partial_{w_1}(B)D_r g^0 - \partial_{w_2}(B)D_r^2 g^0$$
$$- \partial_{w_3}(B)D_r^3 g^0 = 0,$$
$$M_1 g^1 + D_z^1 g^0 + M_2 f^1 = 0, \tag{A7}$$

where

$$M_0 = D_z^0 + vD_r + v_1,$$
$$M_1 = D_z^0 + vD_r + v_1 + v/r,$$
$$M_2 = wD_r + w_1 + w/r. \tag{A8}$$

We now set

$$f^0 = \frac{1}{2}D_r(v^2), \qquad g^0 = \frac{1}{r}D_r(wvr), \tag{A9}$$

following [30]. This choice obviously satisfies zeroth-order equations (A7) and the invariance conditions $f^0 = 0$ and $g^0 = 0$ at the boundary. We can then find f^1 from the first of the first-order equations in (A7), which we rewrite as

$$M_0(f^1 + B) = 0. \tag{A10}$$

The solution of this equation is expressed in terms of invariants of the operator M_0,

$$f^1 = \frac{1}{2}D_r\left(S(\chi) - \rho^2 F - \frac{1}{\sqrt{w}}(\triangle_\perp\sqrt{w})\right), \quad \chi = r - vz \tag{A11}$$

where

$$S(\chi) = \rho^2 F(J) + \frac{1}{\chi\sqrt{J(\chi)}}\partial_\chi[\chi\partial_\chi(\sqrt{J(\chi)})],$$
$$F(J) = 1 - \frac{N_e\{\gamma[J(\chi)]\}}{\gamma[J(\chi)]}. \tag{A12}$$

Substituting this result in the second first-order equation in (A7) leads to an equation for the function g^1:

$$M_1 g^1 + \frac{1}{2r}D_r[wzD_r S(\chi)] = 0. \tag{A13}$$

It is easy to show by direct substitution that Eq. (A13) can be rewritten as

$$M_0(rg^1) + \tfrac{1}{2}D_r[wzD_r S(\chi)] = 0.$$

This equation can be integrated similarly to Eq. (A10). We then obtain

$$rg^1 = -\tfrac{1}{2}D_r(rwz\partial_\chi S).$$

Finally, up to the first order in the small parameter b, the Lie-Bäcklund symmetry operators in the canonical form are

$$f = vv_1 + \frac{1}{2}D_r\left(S(\chi) - \rho^2 F - \frac{1}{\sqrt{w}}(\triangle_\perp\sqrt{w})\right), \tag{A14}$$
$$g = v\left(w_1 + \frac{w}{r}\right) + wv_1$$
$$-\frac{z}{2}\left[w(1 - zv_1)\partial_{\chi\chi}S + \left(w_1 + \frac{w}{r}\right)\partial_\chi S\right]. \tag{A15}$$

In view of (6), we can rewrite (A14) as

$$f = -\partial_z v + (1 - zv_1)\frac{\partial_\chi S}{2}.$$

Together with Eq. (A15), the last equation leads to the two relations

$$v = z\frac{\partial_\chi S}{2}, \tag{A16}$$
$$\partial_z v = (1 - zv_1)\frac{\partial_\chi S}{2}, \tag{A17}$$

which must be satisfied to preserve the invariance requirement $f = 0$ and $g = 0$.

Keeping in mind the relation between the canonical form of the symmetry operator and the point-symmetry group operator [48], we can now write the group symmetry operator:

$$R = \left(1 + \frac{z^2}{2}\partial_{\chi\chi}S\right)\partial_z + \frac{\partial_\chi S}{2}\partial_v + \frac{1}{2}(z\partial_\chi S + vz^2\partial_{\chi\chi}S)\partial_r$$
$$-\frac{wz}{2}\left[\left(1 + \frac{vz}{r}\right)\partial_{\chi\chi}S + \frac{1}{r}\partial_\chi S\right]\partial_w. \tag{A18}$$

Operator (A18) is similar to the one previously obtained in [30] for a collimated beam except that $S(\chi)$ now contains the function F, which describes the laser beam nonlinearity in relativistic plasma. Operator (A18) yields a system of

characteristic equations:

$$\frac{dz}{1+z^2\partial_{\chi\chi}S/2} = \frac{dv}{\partial_\chi S/2} = \frac{d\chi}{-v} = \frac{d\ \ln(wr)}{-z\partial_{\chi\chi}S/2}. \tag{A19}$$

This system of equations can be easily integrated after Eq. (A16) is taken into account. The second and third equations in (A19) give

$$S + (\partial_\chi S)^2\frac{z^2}{4} = S(\mu), \tag{A20}$$

where μ corresponds to the value of χ at the boundary. The third and fourth equations in (A19) yield another invariant $rw/\partial_\chi S$, which gives the dependence of w as

$$w = J(\mu)\frac{\chi}{r}\frac{\partial_{\chi^2}S}{\partial_{\mu^2}S} \tag{A21}$$

in terms of its initial profile $J(\chi)$. Correspondingly, r and χ are related as

$$r = \chi(1+z^2\partial_{\chi^2}S). \tag{A22}$$

In summary, the solutions are represented by the equations

$$v(r,z) = \frac{z}{2}\partial_\chi S, \quad w(r,z) = J(\mu)\frac{\chi}{r}\frac{\partial_{\chi^2}S}{\partial_{\mu^2}S}, \tag{A23}$$

where χ and μ are defined as functions of z and r by the relations

$$r = \chi(1+z^2\partial_{\chi^2}S), \quad S(\mu) = S(\chi) + \frac{z^2}{4}(\partial_\chi S)^2. \tag{A24}$$

These solutions are discussed in detail in Sec. III.

[1] G. A. Askar'yan, Zh. Eksp. Teor. Fiz. **42**, 1567 (1962) [Sov. Phys.–JETP **15**, 1088 (1962)].

[2] A. G. Litvak, Zh. Eksp. Teor. Fiz. **57**, 629 (1969) [Sov. Phys.–JETP **30**, 344 (1970)].

[3] C. E. Max, J. Arons, and A. B. Langdon, Phys. Rev. Lett. **33**, 209 (1974).

[4] A. B. Borisov, A. V. Borovskiy, V. V. Korobkin, A. M. Prokhorov, O. B. Shiryaev, X. M. Shi, T. S. Luk, A. McPherson, J. C. Solem, K. Boyer, and C. K. Rhodes, Phys. Rev. Lett. **68**, 2309 (1992).

[5] G.-Z. Sun, E. Ott, Y. C. Lee, and P. Guzdar, Phys. Fluids **30**, 526 (1987).

[6] A. B. Borisov, A. V. Borovskiy, O. B. Shiryaev, V. V. Korobkin, A. M. Prokhorov, J. C. Solem, T. S. Luk, K. Boyer, and C. K. Rhodes, Phys. Rev. A **45**, 5830 (1992).

[7] K. Krushelnick, A. Ting, C. I. Moore, H. R. Burris, E. Esarey, P. Sprangle, and M. Baine, Phys. Rev. Lett. **78**, 4047 (1997).

[8] P. Sprangle, E. Esarey, J. Krall, and G. Joyce, Phys. Rev. Lett. **69**, 2200 (1992).

[9] P. Mora and T. M. Antonsen, Jr., Phys. Rev. E **53**, R2068(R) (1996).

[10] G. A. Askar'yan, S. V. Bulanov, F. Pegoraro, and A. M. Pukhov, Pis'ma Zh. Eksp. Teor. Fiz. **60**, 240 (1994) [JETP Lett. **60**, 251 (1994)].

[11] M. Borghesi, A. J. MacKinnon, L. Barringer, R. Gaillard, L. A. Gizzi, C. Meyer, O. Willi, A. Pukhov, and J. Meyer-ter-Vehn, Phys. Rev. Lett. **78**, 879 (1997).

[12] T. Tajima and J. M. Dawson, Phys. Rev. Lett. **43**, 267 (1979).

[13] D. Umstadter, S. Y. Chen, A. Maksimchuk, G. Mourou, and R. Wagner, Science **273**, 472 (1996).

[14] G. S. Sarkisov, V. Yu. Bychenkov, V. N. Novikov, V. T. Tikhonchuk, A. Maksimchuk, S.-Y. Chen, R. Wagner, G. Mourou, and D. Umstadter, Phys. Rev. E **59**, 7042 (1999).

[15] S. V. Bulanov, F. Pegoraro, and A. M. Pukhov, Phys. Rev. Lett. **74**, 710 (1995).

[16] N. E. Andreev and L. M. Gorbunov, Sov. Phys. Usp. **42**, 49 (1999).

[17] S. C. Wilks, W. L. Kruer, M. Tabak, and A. B. Langdon, Phys. Rev. Lett. **69**, 1383 (1992).

[18] P. McKenna *et al.*, Laser Part. Beams **26**, 591 (2008).

[19] S. A. Akhmanov, A. P. Sukhorukov, and R. V. Khokhlov, Sov. Phys. Usp. **10**, 609 (1967).

[20] V. N. Lugovoi and A. M. Prokhorov, Sov. Phys. Usp. **16**, 658 (1973).

[21] S. N. Vlasov and V. I. Talanov, *Wave-Self-Focusing* (in Russian) (Institute of Applied Physics, Russian Academy of Sciences, Nizhni Novgorod, 1997).

[22] L. Bergé, Phys. Rep. **303**, 259 (1998).

[23] C. Sulem and P.-L. Sulem, *The Nonlinear Schrödinger Equation: Self-Focusing and Wave Collapse* (Springer, New York, 1999).

[24] R. W. Boyd, S. G. Lukishova, and Y. R. Shen, *Self-Focusing: Past and Present* (Springer, New York, 2009).

[25] A. V. Borovsky, A. L. Galkin, O. B. Shiryaev, and T. Auguste, *Laser Physics at Relativistic Intensities* (Springer, New York, 2003).

[26] F. Cattani, A. Kim, D. Anderson, and M. Lisak, Phys. Rev. E **64**, 016412 (2001).

[27] N. Naseri, W. Rozmus, and D. Pesme, Phys. Plasmas **23**, 113101 (2016).

[28] M. D. Feit, A. M. Komashko, S. L. Musher, A. M. Rubenchik, and S. K. Turitsyn, Phys. Rev. E **57**, 7122 (1998).

[29] B. Hafizi, A. Ting, P. Sprangle, and R. F. Hubbard, Phys. Rev. E **62**, 4120 (2000).

[30] V. F. Kovalev, V. Yu. Bychenkov, and V. T. Tikhonchuk, Phys. Rev. A **61**, 033809 (2000).

[31] V. F. Kovalev, K. I. Popov, and V. Yu. Bychenkov, Zh. Eksp. Teor. Fiz. **141**, 31 (2012) [Sov. Phys.–JETP **114**, 25 (2012)].

[32] V. F. Kovalev and D. V. Shirkov, Sov. Phys. Usp. **51**, 815 (2008).

[33] V. F. Kovalev and V. Yu. Bychenkov, JETP Lett. **107**, 458 (2018).

[34] N. Naseri, S. G. Bochkarev, and W. Rozmus, Phys. Plasmas **17**, 033107 (2010).

[35] P. Sprangle, A. Zigler, and E. Esarey, Appl. Phys. Lett. **38**, 346 (1991).

[36] S. D. Patil, M. V. Takale, V. J. Fulari, D. N. Gupta, and H. Suk, Appl. Phys. B **111**, 1 (2013).

[37] E. Siminos, M. Grech, S. Skupin, T. Schlegel, and V. T. Tikhonchuk, Phys. Rev. E **86**, 056404 (2012).

[38] P. Gibbon, F. Jakober, P. Monot, and T. Auguste, IEEE Trans. Plasma Sci. **34**, 343 (1996).

[39] N. M. Naumova, S. V. Bulanov, K. Nishihara, T. Zh. Esirkepov, and F. Pegoraro, Phys. Rev. E **65**, 045402(R) (2002).

[40] L. Gagnon and P. Winternitz, Phys. Lett. A **134**, 276 (1989); J. Phys. A: Math. Gen. **25**, 4425 (1992); Phys. Rev. A **39**, 296 (1989).

[41] K. Izmaylova and A. Chupakhin, Nelin. Dinam. [Rus. J. Nonlin. Dynamics] **3**, 349 (2007).

[42] S. P. Novikov, S. V. Manakov, S. P. Pitaevskii, and V. E. Zakharov, *Theory of Solitons. The Inverse Scattering Method* (Springer, New York, 1984).

[43] A. B. Borisov, X. Shi, V. B. Karpov, V. V. Korobkin, J. C. Solem, O. B. Shiryaev, A. McPherson, K. Boyer, and C. K. Rhodes, J. Opt. Soc. Am. B **11**, 1941 (1994).

[44] S. Sen, M. A. Varshney, and D. Varshney, ISRN Optics **2013**, 642617 (2013).

[45] A. Pukhov and J. Meyer-ter-Vehn, Phys. Rev. Lett. **76**, 3975 (1996).

[46] A. B. Borisov, J. W. Longworth, K. Boyer, and C. K. Rhodes, Proc. Natl. Acad. Sci. USA **95**, 7854 (1998).

[47] L. M. Chen *et al.*, Phys. Plasmas **14**, 040703 (2007).

[48] N. H. Ibragimov, *CRC Handbook of Lie Group Analysis of Differential Equations* (CRC Press, Boca Raton, 1994–1996).